Effects of optical axis direction on optical path difference and lateral displacement of Savart polariscope*

Zhang Chun-Min(张淳民)†, Ren Wen-Yi(任文艺), and Mu Ting-Kui(穆廷魁)

School of Science, Xi'an Jiaotong University, Xi'an 710049, *China*
MOE Key Labaratory for Nonequilibrium Synthesis and Modulation of Condensed Matter, Xi'an Jiaotong University, Xi'an 710049, *China*

(Received 7 April 2009; revised manuscript received 14 July 2009)

A simple method is applied to calculating the optical path difference (OPD) of a plane parallel uniaxial plate with an arbitrary optical axis direction. Then, the theoretical expressions of the OPD and lateral displacement (LD) of Savart polariscope under non-ideal conditions are obtained exactly. The variations of OPD and LD are simulated, and some important conclusions are obtained when the optical axis directions have an identical tolerance of $\pm 1^\circ$. An application example is given that the tolerances of optical axis directions are gained according to the spectral resolution tolerances of the stationary polarization interference imaging spectrometer (SPIIS). Several approximate formulae are obtained for explaining some conclusions above. The work provides a theoretical guidance for the optic design, crystal processing, installation and debugging, data analysis and spectral reconstruction of the SPIIS.

Keywords: stationary polarization interference imaging spectrometer, Savart polariscope, optical axis, optical path difference

PACC: 4215D, 0765E, 4225K, 4225J

1. Introduction

The polarization interference imaging spectrometer (PIIS) was presented in the mid-1990s and a prototype imaging interferometer called digital array scanned interferometer (DASI) was developed at Washington University in 1996.[1,2] DASI is a stationary spatially modulated interferometer spectrometer. Its advantages include high optical throughput, signal linearity, a large dynamic range, wide spectral region, and spectral fidelity. However, there are two weaknesses with it. First, the remote objects or weak signals cannot be detected in that the slit limits the optical throughput and the signal-to-noise ratio. The second is that the hyperbolic far-field interference fringes are not conducive to spectral reconstruction. The stationary polarization interference imaging spectrometer (SPIIS) based on Savart polariscope was presented by Zhang *et al.* in 2000.[3−8] Compared with DASI, it is ultra-compact, stationary, has a wide field of view and high optical throughput.[9−21]

So far, there have been many reports on the ray tracing in uniaxial crystals[22−27] and calculations for the optical path difference (OPD) and lateral displacement (LD) of Savart polariscope.[28−37] But there is no study regarding the effect of the optical axis direction on the OPD and LD. However, the work on the effect is very important for the imaging quality of the SPIIS because the core part of the SPIIS is Savart polariscope. So the work has great significance for the promotion of the SPIIS.

In the present paper, the effects of the optical axis direction on OPD and LD of Savart polariscope are investigated theoretically. It provides a theoretical guidance for the optic design, crystal processing, installation and debugging, data analysis and spectral reconstruction of the SPIIS. The results will provide a theoretical and practical guide to studying, developing and engineering the PIIS.

2. Theory analysis

2.1. Ray tracing in a plane parallel uniaxial plate

A uniaxial crystal is characterized by a single optical axis and two refractive indices: one is n_o, which

*Project supported by the State Key Program of National Natural Science Foundation of China (Grant No. 40537031), the National Natural Science Foundation of China (Grant No. 40875013), the National Defense Basic Scientific Research Project, China (Grant No. A1420080187), the National High Technology Research and Development Program of China (Grant No. 2006AA12Z152).
†Corresponding author. E-mail: zcm@mail.xjtu.edu.cn
© 2010 Chinese Physical Society and IOP Publishing Ltd

is the ordinary refractive constant index and the other is $n(\theta)$, which varies, according to the direction of the wave normal propagation inside the crystal, between $n_{\rm o}$ and the extraordinary refractive constant index $n_{\rm e}$. In a uniaxial crystal, one incident ray is split up into two rays. One of them, called an ordinary ray (o-ray), satisfies Snell's law of refraction, and calculations of its propagation are the same as those for an isotropic medium. The other, called an extraordinary ray (e-ray), does not satisfy Snell's law of refraction, and calculations of its propagation are slightly more complicated. To solve the problem, one can apply either Maxwell's equations[24,25] or a geometrical approach.[26,27] In the present paper we use the method presented in Shen's paper.[22]

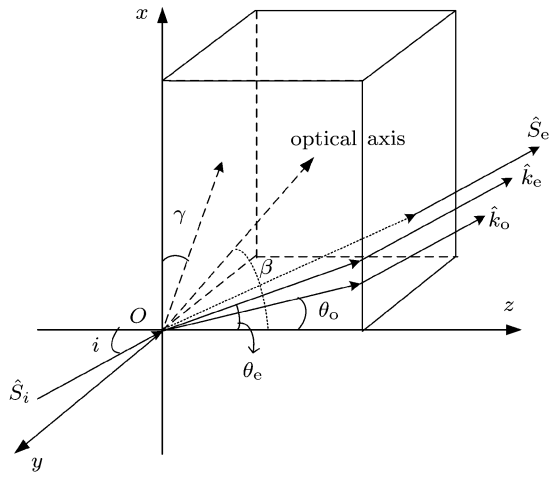


Fig. 1. Illustration of the ray propagation in plane parallel uniaxial plate.

As shown in Fig. 1, we suppose that an incident ray reaches a plane parallel uniaxial plate, where the $\hat{x}\hat{z}$ plane is the incident plane. Reference frame $\hat{x}\hat{y}\hat{z}$ is defined such that $O\hat{x}$ lies along the surface of the plate, $O\hat{z}$ is the inner surface normal, and $O\hat{y}$ completes the right-handed system. The direction of optical axis is determined by angles γ and β together. The angle between $O\hat{z}$ and the optical axis is $0^\circ \le \beta \le 90^\circ$. Correspondingly, γ is the angle measured between the incident surface and the principal section of the uniaxial crystal, and it is within the range of $-180^\circ \le \gamma < 180^\circ$ (observing along $O\hat{z}$, γ is positive when the direction from the positive direction of $O\hat{x}$ to the project of optical axis is clockwise, *vice verse*). Thereby, the direction vector of optical axis can be expressed as

$$\hat{w} = \cos\gamma \sin\beta \hat{x} + \sin\gamma \sin\beta \hat{y} + \cos\beta \hat{z}. \tag{1}$$

2.1.1. The o-wave and o-ray vectors

The o-wave and o-ray vectors obey the Snell's law, and the refractive angles of o-wave and o-ray ($\theta_{\rm o}$) can be calculated from[38]

$$n_i \sin i = n_{\rm o} \sin\theta_{\rm o}, \tag{2}$$

where i is the incident angle, and n_i is the refractive index of incident medium; and the direction vector of incident ray is $\hat{S}_i = \sin i\ \hat{x} + \cos i\ \hat{z}$. Both the incident and refractive waves are in the incident plane,[38] so both the vectors of o-wave and o-ray are

$$\hat{k}_{\rm o} = \hat{S}_{\rm o} = \sin\theta_{\rm o}\hat{x} + \cos\theta_{\rm o}\hat{z}. \tag{3}$$

2.1.2. The e-wave and e-ray vectors

In fact, e-wave and e-ray vectors do not obey Snell's law and they vary with optical axis direction, incident wavelength and refractive medium, etc.[22,27] A simple method used to calculate the e-wave and e-ray is described in Shen's paper.[22] As shown in Fig. 1, the e-wave refractive angle is determined by[22]

$$\tan\theta_{\rm e} = [B + (B^2 + 4AC)^{1/2}]/(2A), \tag{4}$$

where

$$A = n_{\rm o}^2 n_{\rm e}^2 - [n_{\rm o}^2 + (n_{\rm e}^2 - n_{\rm o}^2)\sin^2\beta\cos^2\gamma] n_i^2 \sin^2 i, \tag{5}$$

$$B = (n_{\rm e}^2 - n_{\rm o}^2) n_i^2 \sin^2 i \sin 2\beta \cos\gamma, \tag{6}$$

$$C = (n_{\rm o}^2 \sin^2\beta + n_{\rm e}^2 \cos^2\beta) n_i^2 \sin^2 i. \tag{7}$$

Based on Eqs. (4)–(7), we can obtain

$$\begin{aligned}\cot\theta_{\rm e} &= [(B^2 + 4AC)^{1/2} - B]/(2C) \\ &= \frac{(n_{\rm o}^2 - n_{\rm e}^2)\sin\beta\cos\beta\cos\gamma}{n_{\rm o}^2\sin^2\beta + n_{\rm e}^2\cos^2\beta} \\ &\quad + \frac{n_{\rm o}\{n_{\rm e}^2(n_{\rm o}^2\sin^2\beta + n_{\rm e}^2\cos^2\beta) - [(n_{\rm o}^2 - n_{\rm e}^2)\sin^2\beta\sin^2\gamma + n_{\rm e}^2] n_i^2 \sin^2 i\}^{1/2}}{(n_{\rm o}^2\sin^2\beta + n_{\rm e}^2\cos^2\beta) n_i \sin i}.\end{aligned} \tag{8}$$

The e-wave vector is expressed as

$$\hat{k}_{\rm e} = \sin\theta_{\rm e}\hat{x} + \cos\theta_{\rm e}\hat{z}. \tag{9}$$

According to the relation

$$\cos^{-2}\theta_{\rm e} = 1 + \tan^2\theta_{\rm e}, \tag{10}$$

the angle between e-wave and the optical axis is calculated from

$$\cos\theta = (\cos\beta + \sin\beta\cos\gamma\tan\theta_{\rm e})(1+\tan^2\theta_{\rm e})^{-1/2}. \tag{11}$$

The e-wave refractive index is given by[38]

$$n(\theta) = n_{\rm o}n_{\rm e}(n_{\rm o}^2\sin^2\theta + n_{\rm e}^2\cos^2\theta)^{-1/2}, \tag{12}$$

and $n(\theta)$ can also be expressed as[38]

$$n(\theta) = n_i\sin i/\sin\theta_{\rm e}. \tag{13}$$

In accordance with Shen's paper,[22] the e-ray vector is

$$\begin{aligned}\hat{S}_{\rm e} &= (\xi\sin\theta_{\rm e} + \eta\sin\beta\cos\gamma)\hat{x} + \eta\sin\beta\sin\gamma\hat{y} \\ &\quad + (\xi\cos\theta_{\rm e} + \eta\cos\beta)\hat{z} \\ &= S_x\hat{x} + S_y\hat{y} + S_z\hat{z}.\end{aligned} \tag{14}$$

The normalized direction vector of $\hat{S}_{\rm e}$, denoted by $\hat{S}'_{\rm e}$, is

$$\hat{S}'_{\rm e} = (S_x^2 + S_y^2 + S_z^2)^{-1/2}(S_x\hat{x} + S_y\hat{y} + S_z\hat{z}), \tag{15}$$

where

$$S_x^2 + S_y^2 + S_z^2 = \xi^2[1 + \varepsilon^2 + 2\varepsilon(\sin\beta\cos\gamma\tan\theta_{\rm e} + \cos\beta)(1+\tan^2\theta_{\rm e})^{-1/2}], \tag{16}$$

$$\xi = \frac{n_{\rm o}^2\cos\theta_r}{n_{\rm e}^2\cos\theta} = [1 + (n_{\rm e}^4/n_{\rm o}^4 - 1)\cos^2\theta]^{-1/2}, \tag{17}$$

$$\eta = (1 - n_{\rm o}^2/n_{\rm e}^2)\cos\theta_r = (n_{\rm e}^2/n_{\rm o}^2 - 1)[1 + (n_{\rm e}^4/n_{\rm o}^4 - 1)\cos^2\theta]^{-1/2}\cos\theta, \tag{18}$$

$$\theta_{\rm r} = \arctan\left(\frac{n_{\rm o}^2}{n_{\rm e}^2}\tan\theta\right), \tag{19}$$

and $\theta_{\rm r}$ is the angle between e-ray vector and the optical axis direction vector, and

$$\varepsilon = \eta/\xi = (n_{\rm e}^2/n_{\rm o}^2 - 1)(\cos\beta + \sin\beta\cos\gamma\tan\theta_{\rm e})(1+\tan^2\theta_{\rm e})^{-1/2}. \tag{20}$$

From Eqs. (14) and (2), one can deduce that

$$\begin{aligned}S_x/S_z &= \frac{\sin\theta_{\rm e} + \varepsilon\sin\beta\cos\gamma}{\cos\theta_{\rm e} + \varepsilon\cos\beta} \\ &= \frac{\tan\theta_{\rm e} + (n_{\rm e}^2/n_{\rm o}^2 - 1)(\cos\beta + \sin\beta\cos\gamma\tan\theta_{\rm e})\sin\beta\cos\gamma}{1 + (n_{\rm e}^2/n_{\rm o}^2 - 1)(\cos\beta + \sin\beta\cos\gamma\tan\theta_{\rm e})\cos\beta},\end{aligned} \tag{21}$$

$$\begin{aligned}S_y/S_z &= \frac{\varepsilon\sin\beta\sin\gamma}{(1+\tan^2\theta_{\rm e})^{-1/2} + \varepsilon\cos\beta} \\ &= \frac{(n_{\rm e}^2/n_{\rm o}^2 - 1)(\cos\beta + \sin\beta\cos\gamma\tan\theta_{\rm e})\sin\beta\sin\gamma}{1 + (n_{\rm e}^2/n_{\rm o}^2 - 1)(\cos\beta + \sin\beta\cos\gamma\tan\theta_{\rm e})\cos\beta}.\end{aligned} \tag{22}$$

The angle between the e-wave and e-ray vectors designated by α is given by

$$\alpha = \arccos[(\sin\theta_{\rm e}S_x + \cos\theta_{\rm e}S_z)(S_x^2 + S_y^2 + S_z^2)^{-1/2}]. \tag{23}$$

And the e-ray refractive index is presented by[38]

$$n_{\rm es} = n(\theta)\cos\alpha = n_i\sin i(S_x + S_z/\tan\theta_{\rm e})(S_x^2 + S_y^2 + S_z^2)^{-1/2}. \tag{24}$$

2.1.3. Optical paths of o-ray and e-ray

We assume that the thickness of the plane parallel uniaxial plate is t, the incident point on the front surface of the plate is the origin, and the exit point coordinate of the o-ray is ($X_{\rm o} = t\tan\theta_{\rm o}$, $Y_{\rm o} = 0$, $Z_{\rm o} = t$). Thereby, the optical path of o-ray denoted by $\Delta_{\rm o}$ is

$$\Delta_{\rm o} = n_{\rm o}(X_{\rm o}^2 + 1)^{1/2} = n_{\rm o}t\sec\theta_{\rm o}. \tag{25}$$

The exit point coordinate of the e-ray is ($X_{\rm e} = tS_x/S_z$, $Y_{\rm e} = tS_y/S_z$, $Z_{\rm e} = t$), and we can obtain

$$(X_{\rm e}^2 + Y_{\rm e}^2 + Z_{\rm e}^2)^{1/2} = t(S_x^2 + S_y^2 + S_z^2)^{1/2}/S_z. \tag{26}$$

Therefore, the optical path of e-ray is given by

$$\Delta_{\rm e} = n_{\rm es}(X_{\rm e}^2 + Y_{\rm e}^2 + Z_{\rm e}^2)^{1/2} = tn_i \sin i(S_x/S_z + 1/\tan\theta_{\rm e}). \tag{27}$$

Equation (27) is meaningless because the term $1/\tan\theta_{\rm e}$ is infinite when the incident ray is normally incident ($i = 0°$). Applying the basic formulae in the reference,[22] we obtain

$$\Delta_{\rm e}^{i=0°} = t[(n_{\rm o}^4 \sin^2\beta/n_{\rm e}^2 + n_{\rm e}^2\cos^2\beta)/(\sin^2\beta + n_{\rm e}^2\cos^2\beta/n_{\rm o}^2)]^{1/2}, \tag{28}$$

where $\Delta_{\rm e}^{i=0°}$ is the optical path corresponding to $i = 0°$.

2.2. Principle of Savart polariscope

The optical scheme of Savart polariscope is shown in Fig. 2. It is composed of two identical plane parallel plates of uniaxial negative crystal which are clung together with Canada balsam. The optical axis of the first plate is in the $\hat{x}o\hat{z}$ plane, the angle between the optical axis and $\hat{y}$ axis (or $\hat{z}$ axis) is 45°. The optical axis of the second plate is perpendicular to the first plate and in the $\hat{x}o\hat{y}$ plane, the angle between the optical axis and $\hat{y}$ axis (or $\hat{z}$ axis) is 45°. In the first plate the incident ray is split up into o-ray and e-ray. Similarly, the o-ray and e-ray can be split up into o-ray and e-ray in the second plate, respectively, and the four rays are oo-ray, oe-ray, eo-ray and ee-ray. Since the transmittances of the oo-ray and the oe-ray are approaching to 10^{-3}, even 10^{-4},[39] we just consider the oe-ray and the eo-ray in the SPIIS. The exit rays are parallely laterally sheared but not longitudinally shared. The vibration directions of the oe-ray and the eo-ray are perpendicular to each other. However, they change into two linearly polarized lights whose vibration directions are identical after they have passed through the polarizer P_2. Ultimately, they would form the interferogram and image of objective on focal plane of the imaging lens.

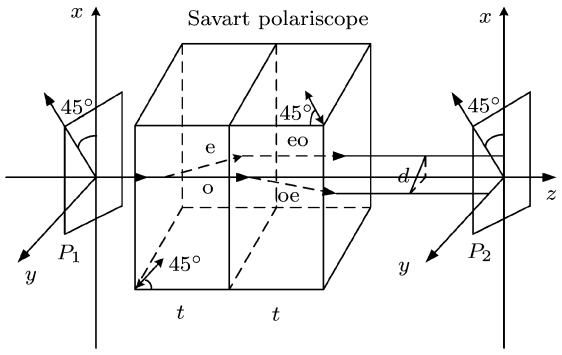


Fig. 2. Structure and optical principle of Savart polariscope.

2.3. OPD and LD of Savart polariscope under non-ideal conditions

As shown in Fig. 3, we assume that the optical axis direction vectors of the two plates in Savart polariscope are, respectively,

$$\hat{w}_1 = \cos\gamma_1 \sin\beta_1\hat{x} + \sin\gamma_1 \sin\beta_1\hat{y} + \cos\beta_1\hat{z}, \tag{29}$$

and

$$\hat{w}_2 = \cos\gamma_2 \sin\beta_2\hat{x} + \sin\gamma_2 \sin\beta_2\hat{y} + \cos\beta_2\hat{z}. \tag{30}$$

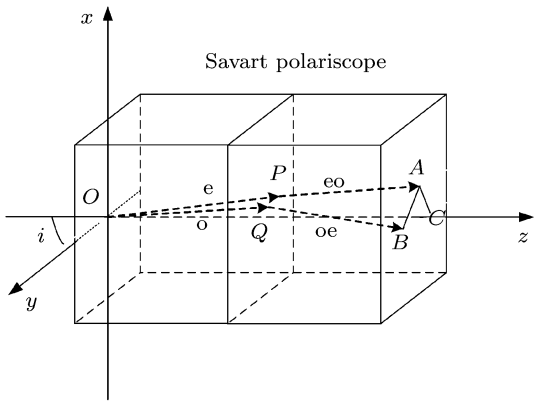


Fig. 3. Description of the optical path difference and lateral displacement for a Savart polariscope under non-ideal condition.

The propagation directions of o-ray and e-ray are parallel in Canada balsam which is isotropic medium, and the refractive indices of o-ray and e-ray are equal. Thereby, the OPD between o-ray and e-ray, induced by Canada balsam, is zero, and the total OPD (Δ) produced by Savart polariscope is

$$\Delta = |\Delta_{\rm e} + \Delta_{\rm eo} - \Delta_{\rm o} - \Delta_{\rm oe} - \Delta_{BC}|\,, \tag{31}$$

where $n_{\rm es}$ and $n_{\rm oes}$ are the ray refractive indices of the e-ray and oe-ray, respectively; $\Delta_{\rm e}$, $\Delta_{\rm eo}$, $\Delta_{\rm o}$, $\Delta_{\rm oe}$, and Δ_{BC} are the optical paths of e-ray, eo-ray, o-ray, oe-ray and BC, they are given as

$$\begin{aligned} &\Delta_{\rm e} = n_{\rm es}\,|OP|\,,\ \ \Delta_{\rm eo} = n_{\rm o}\,|PA|\,,\ \ \Delta_{\rm o} = n_{\rm o}\,|OQ|\,,\\ &\Delta_{\rm oe} = n_{\rm oes}\,|QB|\,,\ \ \Delta_{BC} = n_i\,|BC|\,,\ \ \ |BC| = \boldsymbol{BA}\cdot\boldsymbol{S}_i, \end{aligned} \tag{32}$$

where

$$\boldsymbol{BA} = t(S_{xe}/S_{ze} + \tan\theta_{\rm eo} - S_{xoe}/S_{zoe} - \tan\theta_{\rm o})\hat{x} + t(S_{ye}/S_{ze} - S_{yoe}/S_{zoe})\hat{y}, \tag{33}$$

$$|BC| = |\boldsymbol{BA}\cdot\boldsymbol{S}_i| = t\sin i\,|(S_{xe}/S_{ze} + \tan\theta_{\rm eo} - S_{xoe}/S_{zoe} - \tan\theta_{\rm o})|\,. \tag{34}$$

Using the theory for ray tracing in the plane parallel uniaxial plate, the expression of Δ can be rewritten as

$$\Delta = |\Delta_{\rm e} + \Delta_{\rm eo} - \Delta_{\rm o} - \Delta_{\rm oe} - \Delta_{BC}| = tn_i\sin i\,|\cot\theta_{\rm e} - \cot\theta_{\rm oe}|\,, \tag{35}$$

Substituting Eq. (8) into Eq. (35), the OPD Δ as a function of i, γ_1, β_1, γ_2, β_2 can be obtained, the subscriptions 1 and 2 denote the parameters relevant to the first and the second plates, respectively. When $i = 0^\circ$, the Δ is given by

$$\begin{aligned} \Delta^{i=0^\circ} = t\Big|&[(n_{\rm o}^4\sin^2\beta_1/n_{\rm e}^2 + n_{\rm e}^2\cos^2\beta_1)/(\sin^2\beta_1 + n_{\rm e}^2\cos^2\beta_1/n_{\rm o}^2)]^{1/2}\\ &- [(n_{\rm o}^4\sin^2\beta_2/n_{\rm e}^2 + n_{\rm e}^2\cos^2\beta_2)/(\sin^2\beta_2 + n_{\rm e}^2\cos^2\beta_2/n_{\rm o}^2)]^{1/2}\Big|. \end{aligned} \tag{36}$$

From Eq. (36), we find that only $\Delta^{i=0^\circ}$ is a function of β_1, β_2; and $\Delta^{i=0^\circ} = 0$ when $\beta_1 = \beta_2$. From Eqs. (35) and (36), we find that Δ is just related to the optical paths of the e-ray and oe-ray because the optical paths of o-ray and eo-ray are equal.

Likewise, the lateral displacement d introduced by Savart polariscope is

$$\begin{aligned} d &= (|AB|^2 - |BC|^2)^{1/2}\\ &= t[(S_{xe}/S_{ze} - S_{xoe}/S_{zoe})^2\cos^2 i\\ &\quad + (S_{ye}/S_{ze} - S_{yoe}/S_{zoe})^2]^{1/2}, \end{aligned} \tag{37}$$

where S_{xe}/S_{ze}, S_{xoe}/S_{zoe}, S_{ye}/S_{ze}, and S_{yoe}/S_{zoe} can be calculated from Eqs. (4) and (21). Correspondingly, when $i = 0^\circ$,

$$d^{i=0^\circ} = t[T_1^2 + T_2^2 - 2T_1T_2\cos(\gamma_1 - \gamma_2)]^{1/2}, \tag{38}$$

where

$$T_1 = (1 - n_{\rm o}^2/n_{\rm e}^2)\tan\beta_1/[1 + (n_{\rm o}^2/n_{\rm e}^2)\tan^2\beta_1], \tag{39}$$

$$T_2 = (1 - n_{\rm o}^2/n_{\rm e}^2)\tan\beta_2/[1 + (n_{\rm o}^2/n_{\rm e}^2)\tan^2\beta_2]. \tag{40}$$

From Eqs. (38)–(40), we find that $\gamma_1 - \gamma_2$ is a modulation factor of d.

3. Simulations

In this section, giving the incident angle $i = 3^\circ$, the variations of d and Δ with β_1, γ_1 and β_2, γ_2 will be simulated respectively. Under the ideal condition, the parameter values of Savart polariscope are set as $\gamma_1^{\rm ideal} = 0^\circ$, $\beta_1^{\rm ideal} = 45^\circ$, $\gamma_2^{\rm ideal} = 90^\circ$ and $\beta_2^{\rm ideal} = 45^\circ$. The refractive indices of calcite are $n_{\rm o} = 1.65835$, $n_{\rm e} = 1.48640$ at the wavelength $\lambda = 589.3$ nm. The thickness of a single plate is 6 mm, so the thickness of Savart polariscope is 12 mm. The material between the two plates is Canada balsam whose refractive index ranges approximately from 1.52 to 1.54, and its thickness is negligible. Considering the machining accuracy, we set the variable error tolerances of the optical axis direction angles β_1, γ_1, β_2, γ_2 as $\pm1^\circ$. During the simulation process, the angles β_1 and γ_1 (or β_2 and γ_2) both are variables and the others remain constant.

The effects of β_1 and γ_1 on Δ are depicted in Fig. 4. A useful conclusion that can be obtained from Fig. 4 is that Δ significantly increases with β_1 in a range of $[-1^\circ,\ 1^\circ]$, and increases with γ_1 in a range of $[-1^\circ,\ 0^\circ]$ and decreases in a range of $(0^\circ,\ 1^\circ]$ slightly. So β_1 has a more notable effect on Δ than γ_1 does.

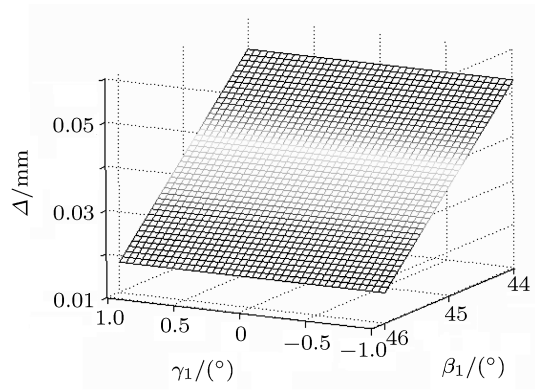


Fig. 4. Optical path difference as a function of γ_1 and β_1 when $i = 3°$.

The effects of β_1 and γ_1 on d are displayed in Fig. 5. Likewise, we can conclude that d decreases with β_1 slightly but decreases with γ_1 obviously. Thereby, the effects of γ_1 upon d are much more prominent than those of β_1.

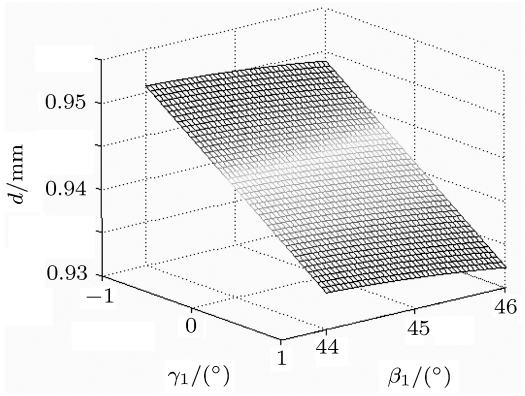


Fig. 5. Lateral displacement as a function of γ_1 and β_1 when $i = 3°$.

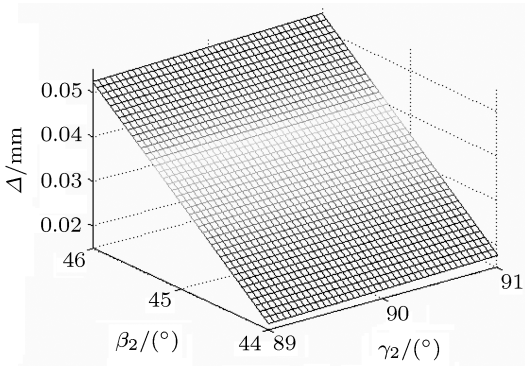


Fig. 6. Optical path difference as a function of γ_2 and β_2 when $i = 3°$.

As shown in Figs. 6 and 7, the angles β_2 and γ_2 also have some effects on Δ and d. From Fig. 6, we can find that Δ increases with β_2 and γ_2. However, the influence of γ_2 on Δ is much less. Based on the analysis in Fig. 7, the useful conclusion that can be drawn is that d quickly increases with γ_2 increasing but slowly decreases with β_2 increasing. Hence, most of effect on d comes from γ_2.

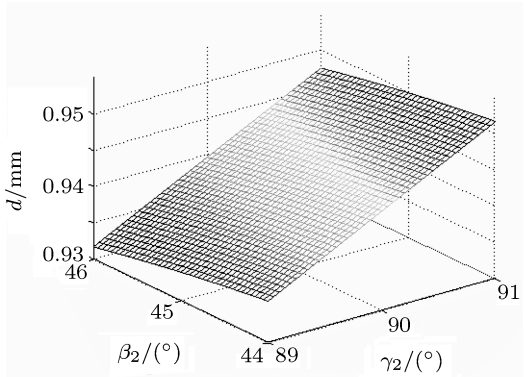


Fig. 7. Lateral displacement as a function of γ_2 and β_2 when $i = 3°$.

4. Application example

We give an application example, in which the matching tolerances of the optical axis direction angles are determined by the tolerance of spectral resolution of the SPIIS. The primary task is that the maximal OPD ($\Delta_{\max}$) should be ascertained before the matching tolerances are gained because the spectral resolution is dictated by $\delta\sigma = (2\Delta_{\max})^{-1}$ in the PIIS.[40] Then the key task is to acquire the relations between $\Delta_{\max}$ and i, β_1, γ_1, β_2, γ_2, in that Δ is a function of them according to Eq. (35).

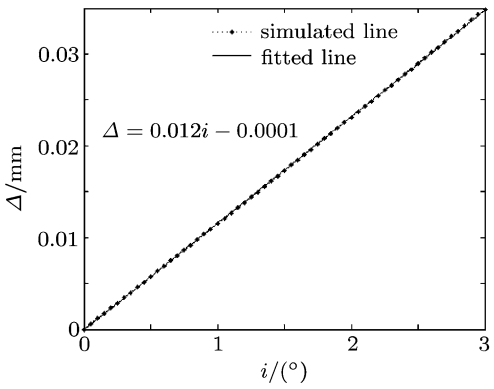


Fig. 8. Optical path difference as a function of i under ideal condition (the solid line: fitted line, the dot line: simulated line).

Figure 8 shows the curve of OPD fluctuating with i under ideal condition. It can obtain the following conclusions: (i) Δ increases with i increasing; (ii) the increase is approximately linear. Through matlab curve fitting, we obtain a linear equation $\Delta = 0.012i - 0.0001$ mm (i is in degree). So we can obtain the maximum OPD $\Delta_{\max}$ when the incident angle i is the maximum (i.e., $i_{\max} = 3°$).

The OPD Δ that varies with i and γ_1 is described in Fig. 9 under non-ideal condition. As can be seen, Δ increases with i increasing when γ_1 is a constant and slightly varies with γ_1 increasing when i is a constant. The OPD Δ approaches to the maximum when the incident angle is the maximum.

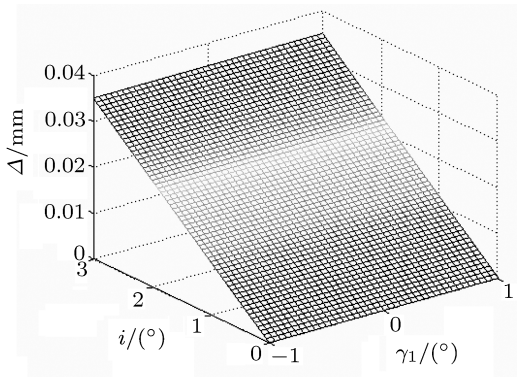


Fig. 9. Optical path difference as a function of i and γ_1.

Figure 10 shows the variations of Δ with i and β_1. We can study it via the two parts as follows: In the first part, the range of β_1 is $[44°,\ 45°)$, the OPD Δ increases with i increasing when β_1 is constant and decreases with β_1 increasing when i is constant. Thereby, Δ also approaches to the maximum when the incident angle is the maximum. In the second part, the range of β_1 is $[45°, 46°]$. From Figs. 10 and 11, we can obtain the conclusions: 1) Δ firstly decreases with i increasing and then increases when β_1 remains constant; 2) Δ increases with β_1 increasing when $i = 0°$ and decreases when $i = 3°$; 3) Δ approximately linearly varies with β_1 when $i = 0°$ and $i = 3°$, and the linear variation relations are $\Delta = 0.018\beta_1 - 0.8$ mm and $\Delta = -0.018\beta_1 + 0.84$ mm (β_1 is in degree), respectively. The two lines representing the simulations each have an intersection when $\beta_1 = 45°58'31''$; 4) when $i \in (0°, 3°)$, the variation of Δ with β_1 is complicated but there appears no peak value. According to the conclusions above, $\Delta_{\max} = \Delta_{i=3°}$ is satisfied for $\beta_1 \in [44°,\ 45°58'31'']$, and $\Delta_{\max} = \Delta_{i=0°}$ holds for $\beta_1 \in (45°58'31'',\ 46°]$.

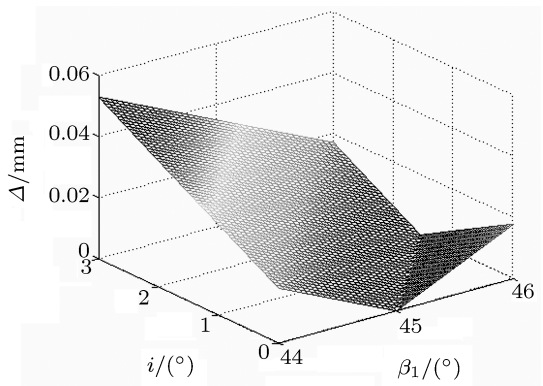


Fig. 10. Optical path difference as a function of i and β_1.

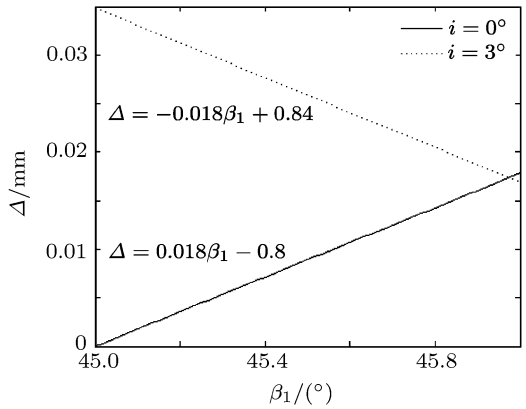


Fig. 11. Comparison between optical path differences as a function of β_1 when $i = 0°$ (solid line), and 3° (dot line) with intersection $\beta_1 = 45°58'31''$.

The conclusions drawn from Fig. 12 are as follows: i) Δ increases with i increasing when γ_2 is constant; ii) Δ increases with γ_2 increasing when i is constant; iii) $\Delta_{\max} = \Delta_{i=3°}$ is satisfied when γ_2 varies from 89° to 91°.

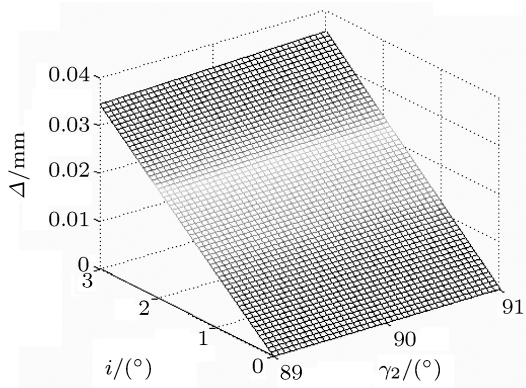


Fig. 12. Optical path difference as a function of i and γ_2.

Figure 13 and 14 show the variations of Δ with i and β_2. What we can obtain from them are as follows: (I) when β_2 is in a range of $[44°, 45°)$, Δ first decreases with i increasing and then increases; (II) Δ varies linearly with β_2 when $i = 0°$ and $i = 3°$. The fitted linear equations are $\Delta = 0.018\beta_2 - 0.8$ mm and $\Delta = 0.018\beta_2 - 0.77$ mm (β_2 is in degree), respectively, and the two fitted lines are parallel with each other; (III) Δ increases with β_2 increasing when

$\beta_2 \in (45°,\ 46°]$; (IV) $\Delta_{\max} = \Delta_{i=3°}$ is satisfied when β_2 varies from 44° to 46°.

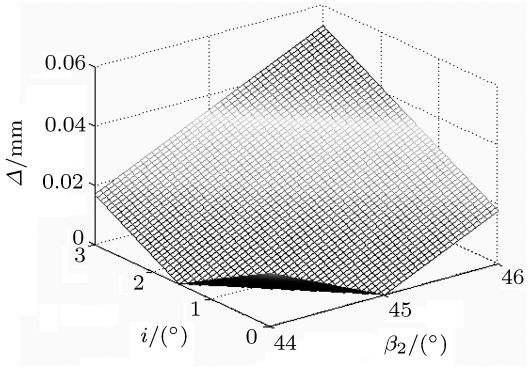


Fig. 13. Optical path difference as a function of i and β_2.

According to this, we can obtain the maximal OPD $\Delta_{\max}^{\text{ideal}} \approx 0.034873$ mm and the spectral resolution $\delta\sigma^{\text{ideal}} = 143.377\ \text{cm}^{-1}$ under ideal condition. Using $\sigma = 1/\lambda$,[40] one can find that

$$\delta\sigma = \delta\lambda/\lambda^2, \tag{41}$$

where σ is wave number. Substituting $\delta\sigma^{\text{ideal}} = 143.377\ \text{cm}^{-1}$ and $\lambda = 589.3$ nm into Eq. (41), we obtain $\delta\lambda^{\text{ideal}} = 4.1286$ nm. The tolerance of $\delta\lambda$ can be represented by $\delta\lambda - \delta\lambda^{\text{ideal}}$, so the relative tolerance of $\delta\lambda$ is $[(\delta\lambda - \delta\lambda^{\text{ideal}})/\delta\lambda^{\text{ideal}}] \times 100\%$. Assume that the relative tolerances are ±1%, ±2%, ±3%, ±4%, ±5% , respectively, then we will have the tolerances of the optical axis direction angles via the conclusions above. Then, a conclusion that can be obtained is that the tolerances of γ_1 and γ_2 are very wide and they are useless for the practical application. Therefore, their exact tolerance should be obtained through other parameters such as d. Listed in Table 1 are the tolerances of β_1 and β_2 for each relative tolerance of spectral resolution. And it is found that the signs of $\delta\beta_1$ and $\delta\beta_2$ are opposite.

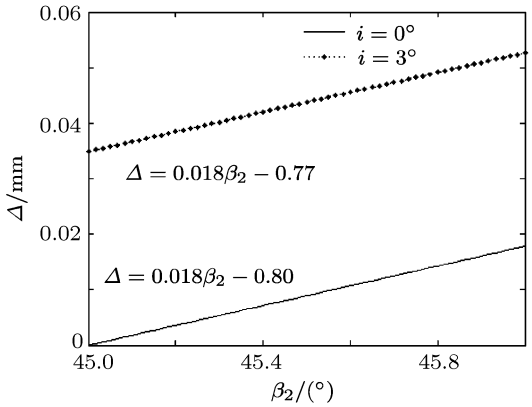


Fig. 14. Comparison between the optical path differences as a function of β_2 when $i = 0°$ (solid line) and 3° (dot line).

Table 1. Tolerances of β_1 and β_2.

$[(\delta\lambda - \delta\lambda^{\text{ideal}})/\delta\lambda^{\text{ideal}}] \times 100\%$	$\delta\lambda - \delta\lambda^{\text{ideal}}$/nm	$\delta\beta_1 = \beta_1 - 45°/(″)$	$\delta\beta_2 = \beta_2 - 45°/(″)$
+1%	+0.0413	+6	−7
−1%	−0.0413	−6	+7
+2%	+0.0825	+13	−14
−2%	−0.0825	−13	+14
+3%	+0.1239	+20	−21
−3%	−0.1239	−21	+21
+4%	+0.1651	+27	−28
−4%	−0.1651	−28	+28
+5%	+0.2064	+34	−34
−5%	−0.2064	−35	+35

5. Discussion

In this section, we will give two formulae to explain part of the conclusions discussed above. Since the maximal incidence angle is 3°, we just reserve the constant terms and the terms in $\sin i$ through Taylor expansions, the approximation expression of Δ can be written as

$$\begin{aligned}\Delta &\approx \Big| tn_{\rm o}n_{\rm e}[(n_{\rm o}^2\sin^2\beta_1 + n_{\rm e}^2\cos^2\beta_1)^{-1/2} - (n_{\rm o}^2\sin^2\beta_2 + n_{\rm e}^2\cos^2\beta_2)^{-1/2}] \\ &\quad + tn_i\sin i(n_{\rm o}^2 - n_{\rm e}^2)\left(\frac{\sin\beta_1\cos\beta_1\cos\gamma_1}{n_{\rm o}^2\sin^2\beta_1 + n_{\rm e}^2\cos^2\beta_1} - \frac{\sin\beta_2\cos\beta_2\cos\gamma_2}{n_{\rm o}^2\sin^2\beta_2 + n_{\rm e}^2\cos^2\beta_2}\right)\Big| \\ &\doteq \Big| tn_{\rm o}n_{\rm e}[(n_{\rm o}^2\sin^2\beta_1 + n_{\rm e}^2\cos^2\beta_1)^{-1/2} - (n_{\rm o}^2\sin^2\beta_2 + n_{\rm e}^2\cos^2\beta_2)^{-1/2}] \\ &\quad + tn_i i(n_{\rm o}^2 - n_{\rm e}^2)\left(\frac{\sin\beta_1\cos\beta_1\cos\gamma_1}{n_{\rm o}^2\sin^2\beta_1 + n_{\rm e}^2\cos^2\beta_1} - \frac{\sin\beta_2\cos\beta_2\cos\gamma_2}{n_{\rm o}^2\sin^2\beta_2 + n_{\rm e}^2\cos^2\beta_2}\right)\Big|. \end{aligned} \tag{42}$$

Based on Eq. (42), we can obtain that: I) when $i = 0$ (normal incidence), $\Delta = 0$ is satisfied just under the condition of $\beta_1 = \beta_2$; II) Δ varies linearly with i approximately.

Rewriting β_1 and β_2 as $\beta_1 = \pi/4 + \delta\beta_1$ and $\beta_2 = \pi/4 + \delta\beta_2$, respectively, and using Taylor expansions, equation (42) can be simplified into

$$\begin{aligned}\Delta \approx \Big| & tn_{\rm o}n_{\rm e}\left(\frac{n_{\rm o}^2 + n_{\rm e}^2}{2}\right)^{-1/2}\left(1 - \frac{n_{\rm o}^2 - n_{\rm e}^2}{n_{\rm o}^2 + n_{\rm e}^2}\right)(\delta\beta_1 - \delta\beta_2) \\ & + tn_i i\frac{n_{\rm o}^2 - n_{\rm e}^2}{n_{\rm o}^2 + n_{\rm e}^2}\left[\cos\gamma_1 - \cos\gamma_2 - 2\frac{n_{\rm o}^2 - n_{\rm e}^2}{n_{\rm o}^2 + n_{\rm e}^2}(\delta\beta_1\cos\gamma_1 - \delta\beta_2\cos\gamma_2)\right]\Big|. \end{aligned} \tag{43}$$

From Eq. (43), we can find that Δ varies linearly with β_1 or β_2 when the tolerances of β_1 and β_2 are both less than $\pm1^\circ$. In Eqs. (42) and (43), the angles are all in radian.

6. Conclusions

We described the principle of beam split of the Savart polariscope, and obtained the exact calculation formula of the optical path of e-ray in a plane parallel uniaxial plate with an arbitrary optical axis direction by a simple tracing method. Then the theoretical expressions of the OPD and LD of Savart polariscope under non-ideal conditions are obtained exactly. By the same method, the special forms of the formulae obtained above are achieved when $i = 0^\circ$. Furthermore, the effects of the optical axis directions on OPD and LD are simulated. Through analysing the formulae and simulations, the important conclusions are obtained as follows.

(i) At normal incidence, $\Delta_{\rm e}$ is a function of β, and Δ is influenced only by β_1 and β_2.

(ii) The Δ is determined only by the OPD between e-ray and oe-ray because the optical paths of the o-ray and eo-ray are equal in Savart polariscope.

(iii) The angles β_1 and β_2 have more obvious effects on Δ than γ_1 and γ_2.

(iv) The angles γ_1 and γ_2 make greater effects on d than β_1 and β_2.

In the application example, the tolerances of β_1 and β_2 are achieved according to the relative spectral resolution tolerance of the SPIIS. We can find that when the relative spectral resolution tolerance is $+1\%$, $\delta\beta_1$ and $\delta\beta_2$ are $+6''$ and $-7''$, respectively; However, when the relative spectral resolution tolerance is -1%, $\delta\beta_1$ and $\delta\beta_2$ are $-6''$ and $+7''$, respectively. The signs of $\delta\beta_1$ and $\delta\beta_2$ are opposite. However, owning to the fact that tolerances of γ_1 and γ_2, which are gained according to the relative spectral resolution tolerances, are far bigger than those of β_1 and β_2, or those of processing technology, they should be obtained through the tolerances of the parameters such as d. In the process of seeking the maximal OPD, we find that Δ varies with i under ideal condition and with β_1 and β_2 under non-ideal condition linearly, and it is explained by the approximate expressions of Δ in Section 5. Thereby, a guiding theoretical foundation is established by the present study for the optic design, crystal processing, installation and debugging, data analysis and spectral reconstruction of the SPIIS.

References

[1] Smith W H and Hammer P D 1996 *Appl. Opt.* **35** 2902

[2] Hammer P D, Valero F P, Peterson D L and Smith W H 1993 *Pro. SPIE* **1937** 244

[3] Zhang C M, Xiang L B and Zhao B C 2000 *Pro. SPIE* **4087** 957

[4] Zhang C M, Xiang L B, Zhao B C and Yuan X J 2002

Opt. Commun. **203** 21
[5] Zhang C M, Zhao B C, Xiang L B and Zha X W 2003 *Opt. Commun.* **227** 221
[6] Zhang C M, Xiang L B and Zhao B C 2004 *J. Opt.* A: *Pure Appl. Opt.* **6** 815
[7] Zhang C M, Zhao B C and Xiang L B 2004 *Appl. Opt.* **43** 6090
[8] Zhang C M, Zhao B C, Xiang L B, Li Y C and Peng Z H 2006 *Pro. SPIE* **6150** 615001
[9] Mu T K, Zhang C M and Zhao B C 2009 *Appl. Opt.* **48** 2333
[10] Zhang C M, Yan X G and Zhao B C 2008 *Opt. Commun.* **281** 2050
[11] Mu T K, Zhang C M and Zhao B C 2009 *Opt. Commun.* **282** 1984
[12] Mu T K, Zhang C M and Zhao B C 2009 *Acta Phys. Sin.* **58** 3877 (in Chinese)
[13] Ren W Y, Zhang C M and Mu T K 2009 *Chin. Phys. Lett.* **26** 084209-1
[14] Mu T K, Zhang C M and Zhao B C 2009 *Opt. Commun.* **282** 1699
[15] Wu L, Zhang C M and Zhao B C 2007 *Opt. Commun.* **273** 67
[16] Zhang C M and He J 2006 *Opt. Express* **14** 12561
[17] Zhang C M, Zhao B C and Xiang L B 2006 *Optik* **117** 261
[18] Zhang C M, Zhao B C, Yuan Z L and Huang W J 2009 *J. Opt.* A: *Pure Appl. Opt.* **11** 085401
[19] Jian X H, Zhang C M and Zhao B C 2007 *Acta Phys. Sin.* **56** 824 (in Chinese)
[20] Yuan Z L, Zhang C M and Zhao B C 2007 *Acta Phys. Sin.* **56** 6413 (in Chinese)
[21] Du J, Zhang C M, Zhao B C and Sun Y 2007 *Acta Phys. Sin.* **57** 6311 (in Chinese)
[22] Shen W M and Shao Z X 2002 *Acta Opt. Sin.* **22** 765 (in Chinese)
[23] Shao Z X and Yi C 1994 *Appl. Opt.* **33** 1209
[24] Simon M C and Echarri R M 1983 *Appl. Opt.* **22** 354
[25] Beyerle G and McDermid I S 1998 *Appl. Opt.* **37** 7947
[26] Swindell W 1975 *Appl. Opt.* **14** 2298
[27] Zhang W Q 1992 *Appl. Opt.* **31** 7328
[28] Wu L, Zhang C M, Yuan Y and Zhao B C 2005 *Acta Opt. Sin.* **25** 885 (in Chinese)
[29] Jian X H, Zhang C M, Sun Y and Wu L 2007 *Acta Opt. Sin.* **27** 643 (in Chinese)
[30] Wu J F, Zhang C M, Zhang Y T, Liu H C and Zhai X J 2008 *Chin. Phys.* B **17** 2504
[31] Mu T K, Zhang C M and Zhao B C 2009 *Acta Phys. Sin.* **58** 3877 (in Chinese)
[32] Mu T K, Zhang C M and Zhao B C 2009 *Opt. Commun.* **282** 1984
[33] Wu H Y, Zhang C M and Zhao B C 2009 *Acta Phys. Sin.* **58** 1642 (in Chinese)
[34] Zhang C M, Liu N and Wu F Q 2010 *Acta Phys. Sin.* **59** (in Chinese)
[35] Zhang C M, Zhu L Y and Zhao B C 2010 *Acta Phys. Sin.* **59** (in Chinese)
[36] Zhang C M, Zhao B C, Yuan Y and He J 2006 *Proc. SPIE* **6032** T320
[37] Zhang C M, Zhao B C, Li Y C and Ye J Y 2007 *Proc. SPIE* **6279** D2791
[38] Born M and Wolf E 1999 *Principles of Optics* 7th ed. (Cambridge: Cambridge University Press) pp. 790–852
[39] Peng Z H, Zhang C M, Zhao B C, Li Y C and Wu F Q 2006 *Acta Phys. Sin.* **55** 6374 (in Chinese)
[40] Bell R J 1972 *Introductory Fourier Transform Spectroscopy* (New York: Academic Press) pp. 23–67